

Geothermal heating and episodic cold-seawater intrusions into an isolated ridge-flank basin near the Mid-Atlantic Ridge

Keir Becker ^{1✉}, Richard E. Thomson ², Earl E. Davis³, Heinrich Villinger ⁴ & C. Geoffrey Wheat ⁵

Six-year records of ocean bottom water temperatures at two locations in an isolated, sedimented deep-water (~4500 m) basin on the western flank of the mid-Atlantic Ridge reveal long periods (months to >1 year) of slow temperature rises punctuated by more rapid (~1 month) cooling events. The temperature rises are consistent with a combination of gradual heating by the geothermal flux through the basin and by diapycnal mixing, while the sharper cooling events indicate displacement of heated bottom waters by incursions of cold, dense bottom water over the deepest part of the sill bounding the basin. Profiles of bottom water temperature, salinity, and oxygen content collected just before and after a cooling event show a distinct change in the water mass suggestive of an incursion of diluted Antarctic Bottom Water from the west. Our results reveal details of a mechanism for the transfer of geothermal heat and bottom water renewal that may be common on mid-ocean ridge flanks.

¹Department of Marine Geosciences, Rosenstiel School of Marine and Atmospheric Science, University of Miami, Miami, FL, USA. ²Institute of Ocean Sciences, Fisheries and Oceans Canada, Sidney, BC, Canada. ³Geological Survey of Canada, Natural Resources Canada, Sidney, BC, Canada. ⁴Department of Geosciences, University of Bremen, Bremen, Germany. ⁵College of Fisheries and Ocean Sciences, University of Alaska Fairbanks, Moss Landing, CA, USA. ✉email: kbecker@rsmas.miami.edu

A number of past studies have presented evidence for an important role for geothermal heating of ocean bottom waters in hydrothermal, biological, and physical oceanographic processes associated with hydrothermal systems in oceanic crust. These have been documented particularly well in closed or semi-restricted axial rift segments on the Mid-Atlantic Ridge^{1,2} and Juan de Fuca Ridge³. They have also been documented in two semi-restricted, well sedimented young ridge-flank systems where geothermal fluxes are high: the eastern flank of the Juan de Fuca Ridge, where there are known off-axis vents at some volcanic edifices not covered by sediments⁴, and the Panama Basin, which encompasses three spreading center segments and young ridge flanks^{5,6}. Buoyancy-driven overturn of geothermally heated bottom waters has been suggested to be an important contributor to the global meridional overturning circulation^{7–10}. There remains debate about the magnitude of the geothermal effects, and detailed time-series records of the process have not been reported to date. Here, we present long-term records (from 2011 to 2017) of bottom-water temperatures in an enclosed, sedimented basin called “North Pond” located on the western flank of the Mid-Atlantic Ridge, along with conductivity-temperature-depth (CTD) profiles collected in the center of the basin during an expedition in 2014. These data show evidence for slow geothermal heating of the deep bottom waters, likely combined with a downward heat flux by diapycnal mixing induced by flow over the rough seafloor topography, that is interrupted at seasonal to interannual time scales by gravity currents delivering cold dense bottom water into the basin from the west. This kind of process may be generally important on the flanks of mid-ocean ridges for the transfer of geothermal heat to, and renewal of, ocean bottom waters. In the North Pond setting, we infer that the gravity currents transport diluted Antarctic Bottom Water (AABW) into the basin, so the results may also have implications for the AABW budget in the western North Atlantic Ocean.

North Pond geological, hydrographic, and geothermal setting.

First mapped and named in 1974¹¹, North Pond is a roughly 8×15 km basement depression filled with sediments up to 200–300 m thick on crust 7–8 million years old located on the western flank of the Mid-Atlantic Ridge at $\sim 23^\circ\text{N}$ (Fig. 1). The basin is elongated in a south-southwest to north-northeast direction, subparallel to the mid-Atlantic Ridge, and is surrounded by thinly sedimented basement topographic highs with patches of exposed basement. The deepest sill is on the southwest side, elevated ~ 100 – 200 m relative to the 4400–4500 m average sedimented seafloor depth within North Pond. A series of deep basins runs from the southwest sill area to the west (Fig. 1) and

represents a deep pathway for cold, dense bottom water to reach as far as North Pond from deeper water to the west. This chain of basins is comparable to the ridge-normal canyons and valleys that cross-cut the western flank of the Mid-Atlantic Ridge in the South Atlantic and have been shown to allow flow of deep waters from the west toward the ridge-crest^{12,13}. In the region west of North Pond, the densest global bottom water mass in the oceans, Antarctic Bottom Water (AABW), has been documented to flow northward to at least 30°N in water depths a few hundred meters deeper than North Pond^{14–16}. Some vertical mixing between the AABW and the overlying North Atlantic Deep Water (NADW) is likely in the deep waters of the North Atlantic at the depth of the North Pond sill at the North Pond latitude¹⁴. In the Kane Fracture Zone ~ 110 km north of North Pond, AABW has been mapped to flow eastward to North Pond longitude at depths as shallow as 4600 m¹⁷.

In the mid-1970s, the Deep Sea Drilling Project cored 576 m of basement near the southeast edge of the pond beneath 92 m of sediment in Hole 395A¹⁸. Since then, North Pond has been revisited multiple times for geophysical surveys and further scientific ocean drilling, and it has now become an important type location for studies of low-temperature ridge-flank hydrothermal circulation in thinly sedimented crust formed at slow spreading rates. Over 100 sediment probe measurements of seafloor heat flux distributed throughout the sediment pond^{19–22} have documented an average heat flux of ~ 40 mW m^{-2} , much less than the ~ 180 – 190 mW m^{-2} predicted by conductive plate cooling models for crust of its age²³. Higher values were measured near the northwest and northern edges of the sediment pond, and two values greater than the predicted value were measured on the slopes of the basin, one below sill depth²⁴. These results, combined with two decades of observations of flow of cold ocean bottom water down Hole 395A into permeable uppermost basement^{25–28}, suggest a vigorous low-temperature lateral circulation system within the permeable section of basement beneath the North Pond sediment cap, generally running from south to north, with advective release probably occurring through the thinly sedimented borders of the sediment pond^{19,20,22,24}.

Since 1997, the North Pond low-temperature ridge-flank hydrothermal circulation has been investigated with four sealed borehole Circulation Obviation Retrofit Kit (CORK) hydrogeological observatories^{29,30} focused primarily on subseafloor pressure and temperature measurements and geomicrobiological sampling from basement formations. Three of the installations^{31,32} provided long time-series measurements of bottom water temperatures using platinum resistance temperature detectors (RTDs) from 2011–2017 that we analyze in this paper. We also utilize CTD data

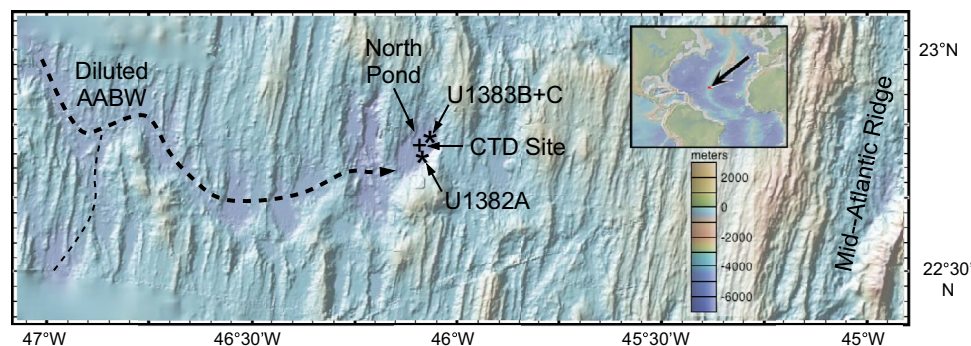


Fig. 1 Location of North Pond in the North Atlantic Ocean and positions of CORKs and CTD casts. Asterisks denote locations of the CORKs; + denotes the position of the two 2014 CTD casts. At the scale of the figure, Holes U1383B and U1383C occupy essentially the same position, labeled U1383B+C. Dashed line denotes pathway for cold dense deep waters inferred to be diluted AABW to reach North Pond from deeper water to the west, passing over the deepest sill on southwest side of North Pond. Base map made with GeoMapApp (www.geomapp.org)⁵⁶.

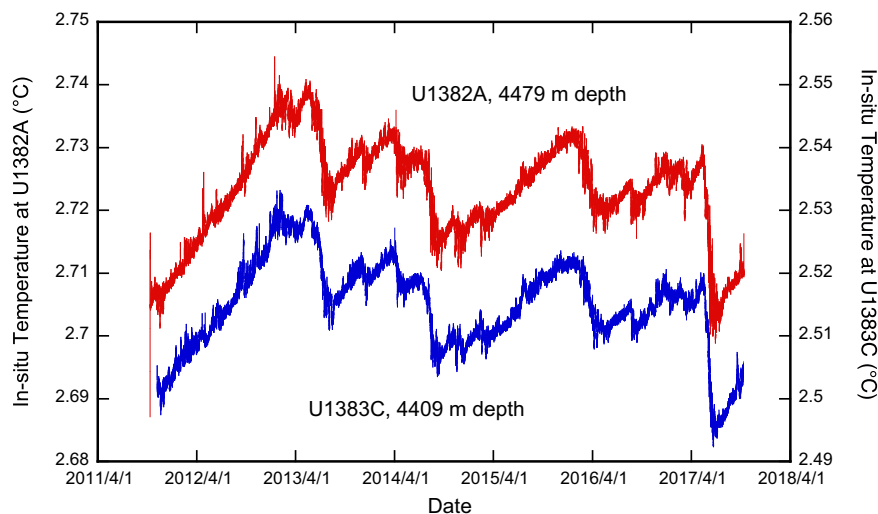


Fig. 2 Six-year records of temporal variability of bottom-water temperatures at Holes U1382A and U1383C. Hole U1382A temperatures are shown in red, Hole U1383C temperatures in blue. As noted in the Methods section, there is an absolute calibration offset between sensors, but relative variations track remarkably well.

collected during a submersible revisit to the CORKs in spring of 2014. Further details are provided in the Methods section.

Results

A: Effects of geothermal heating on North Pond bottom water.

The six-year records of bottom-water in-situ temperatures from the main CORK installations at Holes U1382A and U1383C (Fig. 2) show evidence of a broad range of time scales in North Pond bottom-water temperature variability, with very similar magnitudes and patterns in the temporal variations at the two sites. Because the holes are about 6 km apart, we infer that this is a basin-wide effect. Much of the difference in absolute values of the bottom water temperatures recorded at the two holes is likely due to RTD calibration uncertainties described in the Methods section, but relative variations are resolved much more accurately. In addition, over North Pond there is small adiabatic increase of in-situ seawater temperatures below $\sim 4100 \text{ m}^{24}$ that would produce a difference of in-situ temperature of the order of $0.01 \text{ }^\circ\text{C}$ between the two sites. Nearly identical variations to those at Hole U1383C were also recorded by the temperature sensor in the Hole U1383B data logger located $\sim 25 \text{ m}$ from Hole U1383C, but these are not shown to avoid cluttering Fig. 2.

The general pattern includes long periods (up to $1\frac{1}{2}$ years) of gradual heating, interspersed with abrupt drops in temperature over 2–4 weeks. There appear to be four major episodes of abrupt temperature drops in the record, mainly in late spring or early summer, as well as several smaller drops at other times of the year. The rates of temperature fall average roughly $0.25 \text{ }^\circ\text{C yr}^{-1}$, whereas the rates of temperature rise during the periods of gradual heating average about $0.02 \text{ }^\circ\text{C yr}^{-1}$, over an order of magnitude less (Fig. 2). Using values of $\sim 3870 \text{ J kg}^{-1} \text{ }^\circ\text{C}^{-1}$ for the specific heat, C_p , and $\sim 1048 \text{ kg m}^{-3}$ for the in-situ density, ρ , of North Pond bottom waters calculated from the CTD data described in the next section, the measured warming rate would require a heat input of $\sim 2.6 \text{ mW m}^{-3}$ of heated bottom water.

If we assume horizontally uniform heating within the basin, the time rate of change of temperature, $T(z, t)$, over the depth range, $\Delta z = h$, above the seafloor is given by the one-dimensional heat balance

$$\frac{\partial T}{\partial t} = \frac{(Q_{sf} - Q_h)}{\rho C_p h} \quad (1)$$

where Q_{sf} is the conductive seafloor heat flux, Q_h is the vertical heat flux at elevation, h , above the seafloor, and $\rho C_p = 4.1 \times 10^6 \text{ J }^\circ\text{C}^{-1} \text{ m}^{-3}$. Using (1) and assuming, for now, that there is zero flux from processes within the overlying water column (i.e., $Q_h = 0$), the basin-wide average $Q_{sf} \cong 40 \text{ mW m}^{-2}$ and the observed rate of temperature rise $0.02 \text{ }^\circ\text{C yr}^{-1}$ are consistent with a uniform geothermal heating of the deepest $\sim 15 \text{ m}$ of the basin, easily spanning the depths of the CORK data loggers. However, the average measured conductive flux is almost certainly a lower limit to the total geothermal heating of the bottom waters below the deepest sill depth to the southwest of North Pond, given that it is much less than the predicted plate cooling value of $180\text{--}190 \text{ mW m}^{-2}$. Lateral flow of formation fluids in the permeable basement is likely to advect a significantly greater heat flux to the surrounding thinly sedimented basement exposures surrounding North Pond, where heat can be transferred to the ocean by higher conductive flux and by advection, e.g., as at the locations of two areas of diffuse low-temperature venting respectively on and 3 km from the northwest edge of the sediment pond mapped in 2014²⁴. The salinity of the vented fluids is essentially identical to that of the bottom water because it is a cool seafloor hydrothermal system³³, in which the temperature increase relative to bottom water is small, lateral flow is rapid, and the residence time in the subseafloor is short. At this location, fluids collected from the basement aquifer using the CORKs did not deviate from major ion concentrations in the bottom seawater³⁴. Therefore, any venting fluids in this system will have very little effect on the salinity of the bottom water. Some of the advective flow may be released via surrounding basement highs that are shallower than the North Pond sill depth, so we cannot resolve the true magnitude of the heat that is absorbed by the North Pond bottom waters below sill depth, but an upper limit is provided by applying the total predicted lithospheric heat flux to the region below sill depth at and around North Pond. This would raise the estimate of the thickness, h , of the solely geothermally heated water layer in North Pond by a factor of nearly five, to $h = 70\text{--}75 \text{ m}$.

There is most likely an additional component of heating of the North Pond waters below sill depth by mixing from above, as reported for a $\sim 300 \text{ m}$ thick geothermal boundary layer on the flank of the Juan de Fuca Ridge in Cascadia Basin⁴. Solving (1) for Q_h and assuming spatially uniform diapycnal mixing by breaking

internal waves, shear-instability and other topographically induced processes⁹, the heat flux, Q_{hs} at the sill depth, $h_s = 150$ m (a representative depth for North Pond) that is needed to support uniform heating of 0.02 °C yr⁻¹ within the basin, is given by

$$Q_{hs} = Q_{sf} - (0.02\rho C_p)h_s. \quad (2)$$

For the low-end seafloor heat flux $Q_{sf} = 40$ mW m⁻², the estimated downward heat flux associated with diapycnal mixing, $Q_{hs} = -350$ mW m⁻², while for the more likely high-end seafloor heat flux, $Q_{sf} = 190$ mW m⁻², the estimate for diapycnal mixing decreases to $Q_{hs} = -200$ mW m⁻². Thus, to maintain a temperature rise of 0.02 °C yr⁻¹ throughout the basin requires a downward heat flux from diapycnal mixing that is, at minimum, comparable to the geothermal heating. On the basis of this analysis, we propose that both seafloor heating and diapycnal mixing are contributing significantly to warming of the North Pond water following a cold-water intrusion. Given the uncertainty in the advective geothermal flux into North Pond, we cannot rule out the possibility that diapycnal mixing is more important than geothermal heating but, in any reasonable scenario, it is likely that most of the geothermal heating component would remain trapped in the North Pond bottom waters until there is an influx of cold, dense deep water into the basin.

B. CTD evidence for renewal of North Pond bottom waters in spring 2014. Although none of the four major drops in temperature shown in Fig. 2 occurred during expeditions to the location that conducted CTD casts, there was a smaller fall in temperature observed in early April 2014 between CTD casts on 29 March and 10 April. These casts (Fig. 3a) showed a clear decrease in Conservative Temperature, similar in magnitude to the decrease of in-situ temperature seen in the time series (Fig. 3b), and increases in neutral density and oxygen saturation in the deepest ~ 130 m of the basin up to 4330 m water depth. These observations are all consistent with the interpretation of an influx of cold, dense water over the sill.

Especially noteworthy in the pre-incursion 29 March CTD data are the nearly uniform profile of Conservative Temperature up to the sill depth and a small but significant change in gradient in oxygen saturation at sill depth. The 29 March profile of neutral density is also quite uniform up to sill depth, which is not unexpected given that both salinity and temperature are uniform with depth in the lower layer. In sum, the 29 March profiles indicate that the sill depth marks the upper boundary of the warmed, mixed bottom layer in North Pond prior to the influx of cold, dense bottom water. The 10 April profiles indicate an upward displacement of the warmed, mixed layer by about 25–50 m; however, this may represent a one-time snapshot of a temporally variable response of the structure during the incursion event, but not the post-incursion equilibrium state.

The Absolute Salinity traces show little relative change, except for a slight increase in the bottom part of the 10 April profile that is coincident with the Conservative Temperature decrease below ~ 4330 m water depth. The general offset between the two Absolute Salinity traces (0.004 g kg⁻¹ or roughly one part in 10^4) is within the normal error range for salinity between separate casts. As neutral density and Absolute Salinity both depend mainly on practical salinity and location, the neutral density traces also are offset but we focus here on relative changes, which are well resolved. Between renewal events, North Pond bottom water temperatures are continuously modified by the processes described above and oxygen may be consumed. However, salinity probably remains more constant, except for small increases during any incursions, given that venting low-temperature

hydrothermal fluids are essentially equivalent to bottom seawater as noted above.

The properties of the inflowing waters are likely intermediate between end-member AABW and lower-bound NADW water masses, and would suggest a mixed origin in this instance. The intermediate Conservative Temperature, the elevated dissolved oxygen content, and the location of the site suggest a contribution from AABW that has been found to extend eastward immediately to the west of the North Pond location, with potential temperatures of up to ~ 2 °C¹⁷. In the Discussion, we return to the issue of the identity of the cold intruding water.

Whether the cold-water events are “pulled” or “pushed” is an important distinction to be made³⁵. A “pulled” mechanism was provided by Turner³⁶, who described the release of discrete thermals above a horizontal surface heated from below: “...for most of the time the process of transfer near the boundary is one of conduction, followed by a comparatively short interval during which the conditions are locally restored to the original uniform state by the removal of the buoyant fluid as a plume or thermal.” This might suggest that the buoyant rise of discrete thermals in North Pond pulled in colder bottom water over the bounding sill. However, a more detailed analysis of the records described in the next section strongly suggests a more dynamic “push”, whereby density-driven inflows of colder bottom water flush the deepest waters within North Pond, displacing the heated bottom waters upward.

C: Hydrodynamical processes and gravity current inflows. The thermal records from Holes U1382A and U1383C (Fig. 2) consist of temporal (t) variations in bottom water temperature, $T(t)$, ranging from semi-diurnal (M_2) tidal periods to seasonal and interannual time scales. A correlation analysis of the 6-year records reveals a distinct peak time-lag of ~ 1.6 days between the two sites, with U1382A leading U1383C (Fig. 4a). However, the central peak of the correlation function, $C(\tau)$, as a function of time lag, τ , is quite broad (symmetrical, with a half-width of 7 days) owing to contributions from tidal currents, near-inertial motions, noise, and other processes. Consequently, we undertook a visual examination of the time lags between the two sites on an event-by-event basis (which is straightforward given the limited number of major and intermediate cold-water events) and found a consistent lag of around 2 days, with a few exceptions such as the time difference of 3.4 days for the main event in 2016 (Fig. 4b–d). After adjusting for the average time-lag between the two sites, temperature variations at U1383C track those at U1382A in considerable detail, indicative of a basin-wide response at time scales ranging from days to seasonal.

Based on the strong tidal signals in the temperature records, it is readily apparent that the high frequency temperature variations are caused by currents, \mathbf{u} , that transport the bottom water back and forth past the sensors in the presence of a horizontal temperature gradient, ∇T , with the functional relationship between current and changing water temperature being $\Delta T = (\mathbf{u} \cdot \nabla T)$ for each 2-min time step, Δt . (Thermal sensors can only detect currents where there is a resolvable spatial gradient in water temperature, which means that temperature fluctuations at frequencies higher than primary tidal frequencies are poorly resolved during periods dominated by gradual geothermal warming when the heat is most uniformly distributed in the basin.) Superimposed on the tidally induced variations are large amplitude quasi-annual temperature changes consisting of a slow rise in temperature, followed by abrupt declines in temperature roughly mid-way through the calendar year. This pattern was observed in all years except 2012 and 2015, when there were no major disruptions in temperature rise. The pronounced seasonal

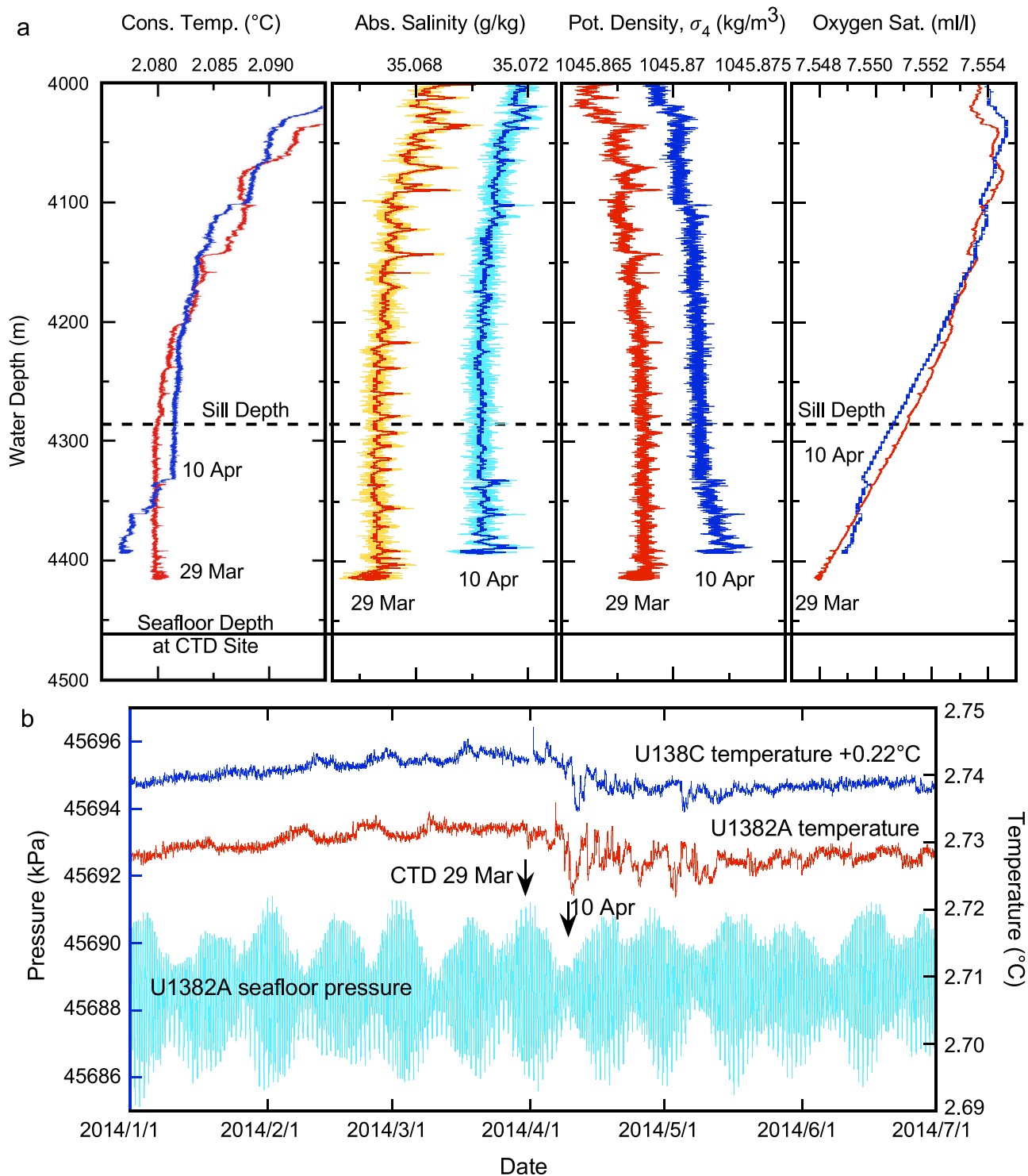


Fig. 3 CTD and seafloor pressure-temperature data spanning the small cooling event of April 2014. This event was clearly registered at both Holes U1382A and U1383C (Fig. 2). **a** Plots of Conservative Temperature, Absolute Salinity, neutral density, and oxygen saturation of bottom waters over North Pond for two CTD casts in 2014 that bracketed the cooling event. Properties from the 29 March CTD cast are shown in red, properties from the 14 April CTD cast in blue. The dark centers of the Absolute Salinity profiles show results of smoothing using a ~ 0.5 m box filter. **b** Expanded record of seafloor pressures recorded at Hole U1382A (cyan) and bottom water in-situ temperatures recorded at Holes U1382A (red) and U1383C (blue) during the first six months of 2014, illustrating the fortnightly (\sim biweekly) cycles in tidal amplitudes in North Pond and the times of the two 2014 CTD casts relative to these cycles.

to interannual variability indicates that the flow dynamics in North Pond are linked to large-scale oceanic circulation processes.

Each major temperature event was followed by smaller amplitude intra-seasonal (3–4 month) fluctuations that mimic

the profile of the longer events. As noted above, temperature increases occurred over durations of several months to over a year at an equivalent heating rate of ~ 0.02 °C yr⁻¹. In contrast, temperature declines had short durations of about a month at an

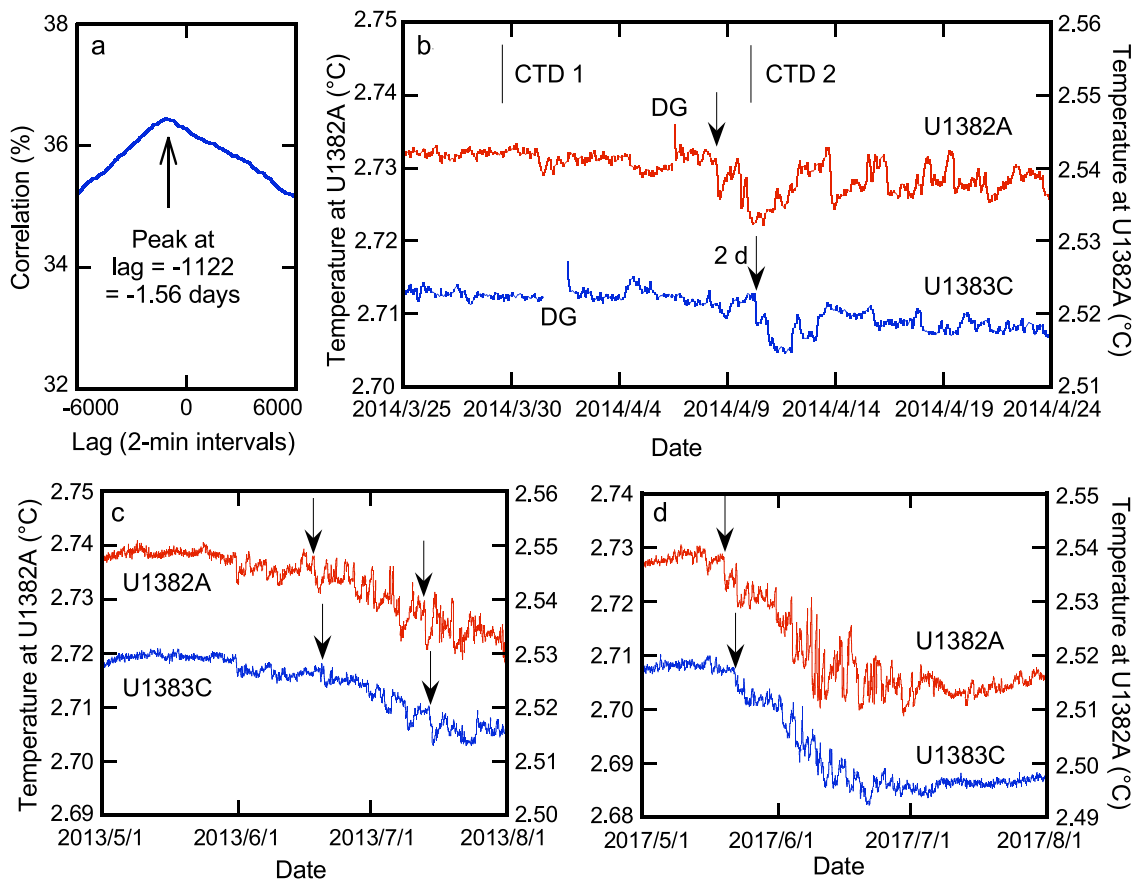


Fig. 4 Correlation function and example time lags between bottom-water temperatures at Holes U1382A and U1383C. **a** The correlation function between temperatures at the two holes as a function of time lag. **b** One month record of in-situ bottom water temperatures at Holes U1382A and U1383C from late March to late April, 2014, spanning the early April cooling event and two CTD casts. DG = data gap on data download, with brief spike on resumption of data logging. **c, d** Expanded three-month views of the major decreases in bottom-water temperatures in 2013 and 2017, respectively, illustrating typical 2- to 3.5-day lags of events at Hole U1383C. In **b-d**, the U1382A temperature record is shown in red, the U1383C record is shown in blue, and vertical arrows indicate example events seen at both locations.

equivalent cooling rate ranging from about $0.20\text{ }^{\circ}\text{C yr}^{-1}$ (2013) to $0.30\text{ }^{\circ}\text{C yr}^{-1}$ (2017). The last recorded decrease in temperature of $0.03\text{ }^{\circ}\text{C}$ in mid-2017 returned the bottom water temperatures to their initial value recorded nearly 6 years earlier. Close examination of the temperature time series during major events (when the flow dynamics are made most apparent because of the formation of a bottom water temperature gradient) also shows temperature modulation at the spring-neap (fortnightly) tidal period of 14-days. The presence of a significant fortnightly period in the tides is confirmed by the bottom pressure records from the basin (Fig. 3b). Thus, bottom water movements in North Pond appear to consist of fortnightly modulated semidiurnal tidal currents on which are superimposed major event-like flows of relatively cold water at intervals of months to years. During major cold-water events, we also observe weaker ~ 7 -day variations in temperature within each fortnightly cycle that appear to be related to the dynamics of the cold-water flows.

Our interpretation of the temperature observations is that they comprise a background state, consisting of extended periods of gradual warming of the bottom water by the seafloor heat flux and diapycnal mixing, that is interrupted by a renewal state, during which the basin is flushed by intrusions of colder, denser bottom water that has spilled over the deepest part of the sill into North Pond from a source farther west on the flank of the Mid Atlantic Ridge (Fig. 5). In this model, bottom water renewal can be triggered once the dense water from the west reaches the elevation

of the deepest gap in the sill in the southwest corner of the basin, and/or once the top of the heated, vertically mixed bottom layer in the North Pond reaches the elevation of the sill. For either mechanism, gravity-driven inflows occur once the density difference between water inside and outside the basin is sufficiently high to establish an inward pressure gradient. Two observational features support the concept of intrusive dense water inflow through the deepest part of the sill at the southwest corner of the basin: (1) all events are first observed at U1382A and then at U1383C 1.5–3.5 days later; and (2) the temperature drops observed at U1382A are considerably greater than at U1383C, indicating that the bottom water mixes with warmer overlying water as it advances slowly from southwest to northeast, or circles in a counterclockwise direction around the bottom of the basin. For example, the initial temperature drop near the beginning of 2016 (Fig. 2) was $0.0077\text{ }^{\circ}\text{C}$ at U1382A but had diminished to $0.0023\text{ }^{\circ}\text{C}$ by the time the density flow reached U1383C about 3.4 days later (average travel speed = 0.02 m s^{-1}). Many short-period events in the temperature decreases can be correlated between U1382A and U1383C (Fig. 4). These typically show lower amplitudes by factors of 2–3 and time lags of a few days at U1383C relative to U1382A. Average travel speeds for the observed time lags of 1.5 to 3.5 days range from 0.046 to 0.020 m s^{-1} , respectively.

The quasi-weekly and quasi-fortnightly modulations of the intrusive events in North Pond are likely caused by variations in

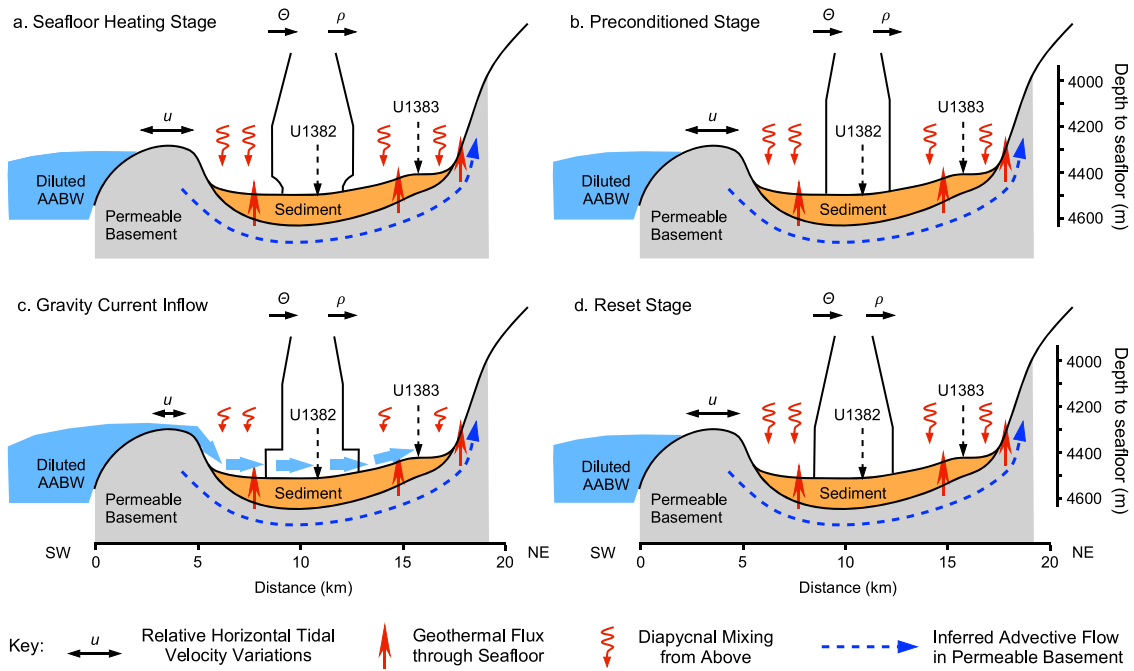


Fig. 5 Cartoon representing four stages of our conceptual model for renewal of North Pond bottom waters. The model involves slow heating of bottom waters by the geothermal flux and diapycnal mixing, setting the stage for cold water intrusions inferred to be from the leading edge of diluted AABW flowing over the deepest sill on the southwest side of North Pond. Plots labeled Θ and ρ represent idealized profiles of Conservative Temperature and density at each stage. Their scales and structures are schematic and intended only to illustrate relative changes in properties with depth. As shown in the bottom key, horizontal two-sided arrows represent relative horizontal tidal velocity variations, red upward arrows represent geothermal heating, red squiggly arrows represent heat input by diapycnal mixing, and dashed blue lines represent inferred low-temperature advective flow within permeable basement. **a** Heating of bottom waters below sill depth by the geothermal flux through the seafloor and by diapycnal mixing in the water column. The curvatures in the profiles in the deepest geothermally heated boundary layer are drawn to be consistent with comparable bottom boundary layers documented in Cascadia Basin⁴. **b** Preconditioned stage reached when the vertical extent of the heated bottom waters reaches sill depth, or slightly shallower. **c** Gravity current inflow stage, when the horizontal tidal velocities over the sill are weak, and colder, denser diluted AABW replaces the deepest bottom water in the basin. **d** Reset stage after the intrusion of diluted AABW and vertical mixing have reestablished near uniform water temperature to sill depth.

tidal current mixing over the deepest portion of the sill leading into the basin from the southwest. As in coastal waterways, density currents readily flow over entrance sills into adjoining basins during neap tides when vertical mixing is weak, but are blocked from crossing the sill during spring tides when vertical mixing is strong^{37,38}. The presence of a weekly signal in the temperature records for the two CORK sites during an intrusion adds further support to the tidal mixing concept in that it indicates that dense-water inflow during neap tides occurs during both the turn to an ebb current and the turn to a flood current. Because the neap tidal currents would be so weak (possibly near zero velocity) during the turns, dense bottom water would have no difficulty slipping over the sill into the adjoining basin at 7-day intervals. Similar processes have been proposed for the density currents observed at 4300 m depth at the southern end of the Middle America Trench off Costa Rica^{39,40}, although in that case, primary forcing originates from equatorial Kelvin waves, and more importantly, turbidity is involved and heat is carried down to deeper levels.

Once the gravity current begins to descend into North Pond, its speed, v_g , would be determined by its thickness, h , the water depth, H , and the density difference, $\Delta\rho$, between the intrusion and the ambient water. For the present case, $H \gg h$, whereby

$$v_g \approx F_r |2g'h|^{1/2} \tag{3}$$

where $g' = g\Delta\rho/\rho$ is reduced gravity, g is the acceleration of gravity, ρ is the density of the ambient bottom water, and F_r is the Froude number (which is of order unity for weakly stratified

fluids³⁹). Using the separation of 6 km between the two sites and the values $h = 50$ m, $\Delta\rho = 0.001 \text{ kg m}^{-3}$, and $\rho = 1048 \text{ kg m}^{-3}$ from the CTD intrusion of April 2014, we obtain a mean gravity current speed of 0.015 m s^{-1} from U1382A to U1383C, which is not inconsistent with the speeds of 0.02 to 0.05 m s^{-1} obtained from the time lags of major intrusive events.

Discussion

In our model, formation of the gravity current intrusions likely results from two factors: (1) seafloor heating and diapycnal mechanical mixing, which warm as much as 200 m of the deepest layer in the basin up to the perimeter of the basin on the southwest side (as indicated by the temperature and density gradients at 4330 m depth in the CTD profiles; Fig. 3a); and (2) the presence of cold, denser bottom water that has shoaled to depths of around 4300 m along the western flank of the ridge. The arrival of dense bottom water outside the sill in late spring and early summer in 4 of the 6 years investigated is clearly related to larger scale processes in the Atlantic Ocean. As noted earlier, the properties of the April 2014 density current and the regional hydrography suggests that the observed inflow consists of AABW (with elevated oxygen and low Conservative Temperature) that had mixed with overlying NADW in the deeper region immediately to the west of the ridge. From geostrophic dynamics, we would expect the Coriolis effect to cause the northward flowing AABW to favor an eastward flow up the ridge flank. In contrast, the southward-flowing NADW would tend to be forced to the west, away from the ridge flank.

If our inference of gravity-driven inflow of modified AABW is correct, then the absence of renewal events in 2012 and 2015 suggests that the AABW source water had not reached as far north and east as North Pond in those two years or was not dense enough to intrude to the bottom of North Pond. In the other four of the six years recorded, there were large-scale intrusions midway through the calendar year that were preceded by one or two shorter duration, smaller amplitude intrusive events; these “precursor” events could indicate that northward and eastward advance of the AABW was still underway. If bottom water temperatures in North Pond are an indicator of the northward flowing AABW, then the leading edge of the water mass was present in 2013, 2014, 2016, and 2017 but not in 2012 and 2015. If this concept is correct, then seasonal to interannual variations in the northward and eastward extent of AABW bottom water over the ridge flank to the west of North Pond could account for the low frequency temperature variations in the basin. This seems consistent with significant interannual variations by a factor of 2–3 in the northward flow of AABW reported over 2009–2011 based on mooring data in deeper water ~ 500 km to the northwest of North Pond⁴¹.

As noted earlier for the Cascadia Basin in the northeast Pacific, heating of the bottom waters by off-axis hydrothermal plumes, the background geothermal flux of ~0.3 W m⁻², and mixing by turbulent motions produces a 250–350 m thick geothermal boundary layer that is clearly observed in CTD data and characterized by reduced vertical stability⁴. Our CTD data from North Pond indicate an analogous geothermal boundary layer up to the deepest sill depth on 29 March 2014, before its displacement by the early April incursion of cold, dense bottom water. Given its very low vertical gradient in neutral density, the section up to roughly 25 to 50 m above sill depth would seem to correspond to the weakly stratified bottom boundary layer as defined for the global ocean⁴². If so, the thickness of that boundary layer would be on the order of 150–250 m above the North Pond seafloor.

Our results do not provide quantitative constraints on the magnitude of the contribution of the geothermal flux from the flank of the Mid-Atlantic Ridge to the global ocean overturning circulation. However, they do document important details of the transfer of the buoyancy arising from geothermal heating to the waters overlying a well-studied basin on the young flank of a slow-spreading ridge, and associated episodes of renewal of basin bottom waters by gravity flows of colder, denser regional bottom waters over the basin sill. That kind of topographic structure is typical on the flanks of slow-spreading ridges in the Atlantic and Indian oceans, so these processes may be common globally. In addition, our interpretation suggests that temporal variations of bottom water properties in North Pond and the series of basins to its west could be diagnostic of the strength of the northward flow of AABW in the North Atlantic west of the Mid-Atlantic Ridge. In that respect, North Pond and basins to its west seem to be intriguing candidates for further temporal monitoring with a more extensive set of instrumentation. This should include arrays of current meters with temperature and salinity sensors, spanning the deepest 200–300 m of the water column, to better delineate the dynamical processes implicated by our limited datasets. Such data could help constrain the degree to which AABW plays a role in the intrusions we have documented, and further elucidate the processes of geothermal heating of the basin bottom waters and their renewal by gravity current intrusions of cold, dense regional bottom waters over basin sills.

Methods

A. CORK bottom-water temperature measurements. The long-term CORK hydrological observatories are designed mainly to sample and monitor seafloor state and hydrological processes. The configurations of the CORKs installed from the scientific drillship JOIDES Resolution in Holes U1382A and U1383C and

“CORK-Lite” deployed in Hole U1383B by remotely operated vehicle (ROV) are described in detail elsewhere^{31,32}. For the installations at Holes U1382A and U1383C, the primary CORK pressure and temperature data loggers are mounted ~4 m above seafloor, or at water depths of ~4479 m at Site U1382 and ~4409 m at Site U1383 (Fig. 1b). Hole U1383B lies ~25 m from Hole U1383C, and its data logger lies about 2.5 m above seafloor. All three data loggers include RTD temperature sensors thermally coupled to the endcaps of the pressure cases that were sampled at 2-minute intervals to provide the long-term 2011–2017 records of bottom water temperatures used in this paper. Data were recovered from data logger memory to a shipboard computer during ROV operations in 2012, 2014, and 2017. Offsets among the RTD readings almost certainly resulted from calibration errors, as calibrations before deployment were done only in an ice bath and at room-temperature, but resolution of relative temporal variations is 0.001 °C in our measurement range. Data logger clock drifts were assessed at the times of the ROV data recovery operations and the clocks were re-synchronized with UTC in 2014 and 2017. Clock drifts averaged ~1–2 min yr⁻¹, with very similar values at Sites U1382A and U1383C, so they are not significant to the findings reported here. At the end of 2017 ROV operations, the data logger memories were cleared and the sample intervals were changed to 20 min, such that sufficient battery power remained for at least a decade more of continued recording of signals such as the bottom water temperature variations reported here.

B. CTD data. The 2014 CTD data used in this study were obtained with a Sea-Bird SBE 9plus CTD profiler using factory calibrations. It included redundant sensors for temperature and conductivity; for each of those parameters, the redundant sensor readings were quite consistent. The lowering speeds and sampling frequency resulted in a data sample every ~0.03 m, so some of the data shown in Fig. 3a were smoothed using a ~0.5 m box filter. The CTD data were processed using the TEOS-10 Gibbs Seawater toolkit⁴³ to produce the profiles of Conservative Temperature and Absolute Salinity shown in Fig. 3a and the values of specific heat and density used in the Results section A. To produce the neutral density profile in Fig. 3a, the data were processed using the legacy EOS-80 neutral density function⁴⁴.

Data availability

Long-term temperature and pressure data from the CORK installations at Holes U1382A, U1383B, and U1383C are freely available from the Marine Geoscience Data System (MGDS)^{45–50} at www.marine-geo.org. North Pond CTD data from 2014 used in this paper are available from PANGAEA^{51,52} at www.pangaea.de. Earlier CTD data from North Pond collected in 2009 and 2012 are also available from PANGAEA^{53–55}. Further CTD data from North Pond collected in 2017 are available via the Biological and Chemical Oceanography Data Management Office at <https://www.bco-dmo.org/dataset-deployment/757723>.

Received: 18 April 2021; Accepted: 7 October 2021;

Published online: 29 October 2021

References

- Murton, B. J., Redbourn, L. J., German, C. R. & Baker, E. T. Sources and fluxes of hydrothermal heat, chemicals and biology within a segment of the Mid-Atlantic Ridge. *Earth Planet. Sci. Lett.* **171**, 301–317 (1999).
- Thurnherr, A. M., Richards, K. J., German, C. R., Lane-Serff, G. F. & Speer, K. G. Flow and mixing in the rift valley of the Mid-Atlantic Ridge. *J. Phys. Ocean.* **32**, 1763–1778 (2002).
- Thomson, R. E. et al. Constrained circulation at Endeavour ridge facilitates colonization by vent larvae. *Nature* **424**, 545–549 (2003).
- Thomson, R. E., Davis, E. E. & Burd, B. J. Hydrothermal venting and geothermal heating in Cascadia Basin. *J. Geophys. Res.* **100**, 6121–6141 (1995).
- Banyte, D. et al. Geothermal heating in the Panama Basin: I. Hydrography of the basin. *J. Geophys. Res. Oceans* **123**, 7383–7392 (2018a).
- Banyte, D. et al. Geothermal heating in the Panama Basin. Part II: Abyssal water mass transformation. *J. Geophys. Res. Oceans* **123**, 7393–7406 (2018b).
- Adcroft, A., Scott, J. R. & Marotzke, J. Impact of geothermal heating on the global ocean circulation. *Geophys. Res. Lett.* **28**, 1735–1738 (2001).
- Hofmann, M. & Maqueda, M. A. Geothermal heat flux and its influence on the oceanic abyssal circulation and radiocarbon distribution. *Geophys. Res. Lett.* **36**, L03603 (2009).
- Emile-Geay, J. & Madec, G. Geothermal heating, diapycnal mixing and the abyssal circulation. *Ocean Sci.* **5**, 203–217 (2009).
- De Lavergne, C., Madec, G., Le Sommer, J., George Nurser, A. J. & Naveira Garabato, A. C. On the consumption of Antarctic bottom water in the abyssal ocean. *J. Phys. Ocean.* **46**, 635–661 (2016).
- Hussong, D. M., Fryer, P. B., Tuthill, J. D. & Wiperman, L. K. The geological and geophysical setting near DSDP Site 395, North Atlantic Ocean. *Init. Repts. DSDP* **45**, 23–27 (1978).

12. Thurnherr, A. M., St. Laurent, L. C., Speer, K. G., Toole, J. M. & Ledwell, J. R. Mixing associated with sills in a canyon on the midocean ridge flank. *J. Phys. Ocean.* **35**, 1370–1381 (2005).
13. Thurnherr, A. M., Clement, L., St. Laurent, L., Ferrari, R. & Ijichi, T. Transformation and upwelling of bottom water in fracture zone valleys. *J. Phys. Ocean.* **50**, 715–726 (2020).
14. Johnson, G. Quantifying Antarctic bottom water and North Atlantic deep water volumes. *J. Geophys. Res.* **113**, C05027 (2008).
15. Morozov, E. G., Tarakanov, R. Y. & Zenk, W. Spreading of Antarctic bottom water in the Atlantic Ocean. *Geogr. Environ. Sustain.* **5**, 24–33 (2012).
16. Frajka-Williams, E., Cunningham, S. A., Bryden, H. & King, B. A. Variability of Antarctic bottom water at 24.5°N in the Atlantic. *J. Geophys. Res.* **116**, C11026 (2011).
17. Morozov, E. G., Tarakanov, R. Y., Frey, D. I., Demidova, T. A. & Makrenko, N. I. Bottom water flows in the tropical fractures of the northern Mid-Atlantic Ridge. *J. Oceanogr.* **74**, 147–167 (2018).
18. Shipboard Scientific Party. Site 395: 23°N, Mid-Atlantic Ridge. *Init. Repts. DSDP* **45**, 131–264 (1978).
19. Langseth, M. G., Hyndman, R. D., Becker, K., Hickman, S. H. & Salisbury, M. H. The hydrogeological regime of isolated sediment ponds in mid-oceanic ridges. *Init. Repts. DSDP* **78B**, 825–837 (1984).
20. Langseth, M. G., Becker, K., Von Herzen, R. P. & Schultheiss, P. Heat and fluid flux through sediment on the western flank of the Mid-Atlantic Ridge: a hydrogeological study of North Pond. *Geophys. Res. Lett.* **19**, 517–520 (1992).
21. Langseth, M. G., Von Herzen, R. P., Becker, K., Müller, P. & Villinger, H. Heat flux in sedimented ponds, MAR-flanks 22–24°N, RV Atlantis II 123-2, 1989. PANGAEA, <https://doi.org/10.1594/PANGAEA.896168> (2018).
22. Schmidt-Schierhorn, F., Kaul, N., Stephan, S. & Villinger, H. Geophysical site survey results from North Pond (Mid-Atlantic Ridge). *Proc. IODP*, **336** <https://doi.org/10.2204/iodp.proc.336.107.2012> (2012).
23. Hasterok, D. A heat flow based cooling model for tectonic plates. *Earth Planet. Sci. Lett.* **361**, 34–43 (2013).
24. Villinger, H. W. et al. Evidence for low-temperature diffuse venting at North Pond, western flank of the Mid-Atlantic Ridge. *Geochem. Geophys. Geosyst.* **20**, 2572–2584 (2019).
25. Becker, K., Langseth, M. G. & Hyndman, R. D. Temperature measurements in Hole 395A. *Leg 78B. Init. Repts. DSDP* **78B**, 689–698 (1984).
26. Kopietz, J., Becker, K. & Hamano, Y. Temperature measurements in Hole 395A, Leg 109. *Proc. ODP, Sci. Results* **109**, 197–203 (1990).
27. Gable, R., Morin, R. H. & Becker, K. Geothermal state of DSDP Holes 333A, 395A, and 534A: results from the Dianaut program. *Geophys. Res. Lett.* **19**, 505–508 (1992).
28. Morin, R. H., Hess, A. E. & Becker, K. In situ measurements of fluid flow in DSDP Holes 395A and 534A: results from the DIANAUT program. *Geophys. Res. Lett.* **19**, 509–512 (1992).
29. Becker, K. & Davis, E. E. A review of CORK designs and operations during the Ocean Drilling Program. *Proc. IODP*, **301**, <https://doi.org/10.2204/iodp.proc.301.104.2005> (2005).
30. Davis, E. E., Becker, K., Kyo, M. & Kimura, T. Foundational experiences and recent advances in long-term deep-ocean borehole observatories for hydrologic, geodetic, and seismic monitoring. *Mar. Tech. Soc. J.* **52**, 74–86 (2018).
31. Edwards, K. J. et al. Design and deployment of borehole observatories and experiments during IODP Expedition 336, Mid-Atlantic Ridge flank at North Pond. *Proc. IODP*, **336**, <https://doi.org/10.2204/iodp.proc.336.109.2012> (2012).
32. Wheat, C. G. et al. CORK-Lite: bringing legacy boreholes back to life. *Sci. Drilling* **14**, 39–43 (2012).
33. Wheat, C. G., Fisher, A. T., McManus, J., Hulme, S. M. & Orcutt, B. N. Cool seafloor hydrothermal springs reveal global geochemical fluxes. *Earth Plan. Sci. Lett.* **476**, 179–188 (2017).
34. Wheat, C. G. et al. Subseafloor cross-hole tracer experiment reveals hydrologic properties, heterogeneities, and reactions in slow-spreading oceanic crust. *Geochem. Geophys. Geosyst.* **21**, e2019GC008804, <https://doi.org/10.1029/2019GC008804> (2020).
35. Gargett, A. Is the thermohaline circulation “pushed” or “pulled”? *Ocean Modelling* **78**, 10–13 (1988).
36. Turner, J. S. *Buoyancy Effects in Fluids* (Cambridge Univ. Press, 1973).
37. Griffin, D. A. & LeBlond, P. H. Estuary/ocean exchange controlled by spring-neap tidal mixing. *Est. Coast. Shelf Sci.* **30**, 275–297 (1990).
38. Thomson, R. E., Kulikov, E. A., Spear, D. J., Johannessen, S. C. & Wills, W. P. A role for gravity currents in cross-sill estuarine exchange and subsurface inflow to the southern Strait of Georgia. *J. Geophys. Res. Oceans* **125**, <https://doi.org/10.1029/2019JC015374> (2020).
39. Thomson, R. E., Davis, E. E., Heesemann, M. & Villinger, H. Observations of long-duration episodic bottom currents in the Middle America Trench: evidence for tidally initiated turbidity flows. *J. Geophys. Res. Oceans* **115**, <https://doi.org/10.1029/2010JC006166> (2010).
40. Thomson, R. E. & Davis, E. E. Equatorial Kelvin waves generated in the western tropical Pacific Ocean trigger mass and heat transport deep within the Middle America Trench off Costa Rica. *J. Geophys. Res. Oceans* <https://doi.org/10.1002/2017JC012848> (2017).
41. McCarthy, G. D. et al. Measuring the Atlantic meridional overturning circulation at 26°N. *Progress Oceanogr.* **130**, 91–111 (2015).
42. Banyte, D., Smeed, D. A. & Maqueda, M. A. The weakly stratified bottom boundary layer of the global ocean. *J. Geophys. Res.* **123**, 5587–5598 (2018).
43. I. O. C., SCOR and IAPSO. The international thermodynamic equation of seawater – 2010: Calculation and use of thermodynamic properties. Intergovernmental Oceanographic Commission, Manuals and Guides No. 56, UNESCO (2010).
44. Jackett, D. R. & McDougall, T. J. A neutral density variable for the world’s oceans. *J. Phys. Ocean.* **27**, 237–263 (1997).
45. Becker, K., Villinger, H. & Davis, E. CORK-II Pressure Data from Hole U1382A along the western flank of the Mid-Atlantic Ridge (2011–2014). IEDA. <https://doi.org/10.1594/IEDA/322273> (2015).
46. Becker, K., Villinger, H. & Davis, E. CORK-II Pressure Data from Hole U1383C along the western flank of the Mid-Atlantic Ridge (2011–2014). IEDA. <https://doi.org/10.1594/IEDA/322274> (2015).
47. Becker, K., Villinger, H., Davis, E. & Wheat, G. CORK-Lite Pressure Data from Hole U1383B along the western flank of the Mid-Atlantic Ridge (2012–2014). IEDA. <https://doi.org/10.1594/IEDA/322275> (2015).
48. Becker, K., Villinger, H. & Davis, E. CORK-II Pressure Data from Hole U1382A along the western flank of the Mid-Atlantic Ridge (2014–2017). IEDA. <https://doi.org/10.1594/IEDA/324535> (2018).
49. Becker, K., Villinger, H. & Davis, E. CORK-II Pressure Data from Hole U1383C along the western flank of the Mid-Atlantic Ridge (2014–2017). IEDA. <https://doi.org/10.1594/IEDA/324536> (2018).
50. Becker, K., Villinger, H., Davis, E. & Wheat, G. CORK-Lite Pressure Data from Hole U1383B along the western flank of the Mid-Atlantic Ridge (2014–2017). IEDA. <https://doi.org/10.1594/IEDA/324537> (2018).
51. Villinger, H. Physical oceanography raw data from CTD cast MSM37_324-1. Department of Geosciences, Bremen University, PANGAEA, <https://doi.org/10.1594/PANGAEA.889809> (2018).
52. Villinger, H. Physical oceanography raw data from CTD cast MSM37_339-1. Department of Geosciences, Bremen University, PANGAEA, <https://doi.org/10.1594/PANGAEA.889814> (2018).
53. Villinger, H. Physical oceanography raw data from CTD cast MSM11/1_379-1. Department of Geosciences, Bremen University, PANGAEA, <https://doi.org/10.1594/PANGAEA.889857> (2018).
54. Villinger, H. Physical oceanography raw data from CTD cast MSM20/5_187_2. Department of Geosciences, Bremen University, PANGAEA, <https://doi.org/10.1594/PANGAEA.889806> (2018).
55. Villinger, H. Physical oceanography raw data from CTD cast MSM20/5_175_1. Department of Geosciences, Bremen University, PANGAEA, <https://doi.org/10.1594/PANGAEA.889805> (2018).
56. Ryan, W. B. F. et al. Global Multi-Resolution Topography (GMRT) synthesis data set. *Geochem. Geophys. Geosyst.* **10**, Q03014 (2009).

Acknowledgements

We thank the following for financial support of the 2011–2017 CORK installations and submersible revisits: (1) the Moore Foundation for financial support via the University of Southern California for much of the hardware costs for the CORKs, (2) the US National Science Foundation for financial support of the pressure and temperature instrumentation on the CORKs (grants OCE-0946795 and OCE-1060855 to KB) and submersible revisits with the ROV Jason (grants OCE-1536623 to CGW and OCE-1536601 to KB), and (3) the Deutsche Forschungsgemeinschaft (German Research Foundation) for R/V Maria S. Merian shiptime in support of 2012 and 2014 submersible operations to the CORKs. We also thank the officers and crews of D/V JOIDES Resolution, R/V Maria S. Merian, R/V Atlantis, and the Jason ROV team for exceptional support of the installations and subsequent submersible operations. Lastly, we are most grateful to the three anonymous reviewers for their highly informative and positive comments and suggestions.

Author contributions

All five co-authors participated actively in writing this report. K.B. led the efforts (a) to obtain funding for and then install the North Pond CORK pressure and temperature instrumentation, (b) to acquire CORK pressure and temperature data during subsequent submersible operations, and (c) to write this contribution. R.E.T. was principal author of Part C of the Results section of this paper. E.E.D. led the construction of the CORK pressure and temperature instrumentation. H.V. obtained funding for and led the 2014 Maria S. Merian cruises that acquired CORK data and supplied the 2014 CTD data used in this paper. C.G.W. led the effort to deploy the “CORK-Lite” in Hole U1383B and first pointed out to K.B. the patterns in North Pond bottom water temperatures as seen in geochemical samplers from 2012–2014.

Competing interests

The authors declare no competing interests.

Additional information

Correspondence and requests for materials should be addressed to Keir Becker.

Peer review information *Communications Earth & Environment* thanks Casimir de Lavergne and the other, anonymous, reviewer(s) for their contribution to the peer review of this work. Primary Handling Editors: Clare Davis.

Reprints and permission information is available at <http://www.nature.com/reprints>

Publisher's note Springer Nature remains neutral with regard to jurisdictional claims in published maps and institutional affiliations.



Open Access This article is licensed under a Creative Commons Attribution 4.0 International License, which permits use, sharing, adaptation, distribution and reproduction in any medium or format, as long as you give appropriate credit to the original author(s) and the source, provide a link to the Creative Commons license, and indicate if changes were made. The images or other third party material in this article are included in the article's Creative Commons license, unless indicated otherwise in a credit line to the material. If material is not included in the article's Creative Commons license and your intended use is not permitted by statutory regulation or exceeds the permitted use, you will need to obtain permission directly from the copyright holder. To view a copy of this license, visit <http://creativecommons.org/licenses/by/4.0/>.

© The Author(s) 2021